Pure Silica Large Pore Zeolite ITQ-7: Synthetic Strategies, Structure-Directing Effects, and Control and Nature of Structural Disorder

L. A. Villaescusa,[†] I. Díaz,[‡] P. A. Barrett,[§] S. Nair,[||] J. M. LLoris-Cormano,[⊥] R. Martínez-Mañez,[†] M. Tsapatsis,[⊗] Z. Liu,[○] O. Terasaki,[#] and M. A. Camblor*[,▽]

Instituto de Química Molecular Aplicada, Departamento de Química, Universidad Politécnica de Valencia, Camino de Vera s/n, 46022 Valencia, Spain, Instituto de Catálisis y Petroleoquímica, Consejo Superior de Investigaciones Científicas (CSIC), C/Marie Curie 2, Campus Cantoblanco, 28049 Madrid, Spain, Praxair, Incorporated, 175 East Park Drive, P.O. Box 44, Tonawanda, New York 14150-7891, School of Chemical & Biomolecular Engineering, Georgia Institute of Technology, 311 Ferst Drive NW, Atlanta, Georgia 30332-0100, AIDICO, València Parc Tecnològic, Avda. Benjamín Franklin 17, Paterna, 46980 Valencia, Spain, Department of Chemical Engineering and Materials Science, University of Minnesota, 421 Washington Avenue SE, Minneapolis, Minnesota 55455, Research Center for Advanced Carbon Materials, National Institute of Advanced Industrial Science and Technology (AIST), Higashi 1-1-1, Tsukuba 305-8565, Japan, Structural Chemistry, Arrhenius Laboratory, Stockholm University, 10691 Stockholm, Sweden, and Instituto de Ciencia de Materiales de Madrid, Consejo Superior de Investigaciones Científicas (CSIC), C/Sor Juana Inés de la Cruz, Campus Cantoblanco, 28049 Madrid, Spain

Received September 18, 2006. Revised Manuscript Received January 8, 2007

Several organic cations derived from the same rigid bicyclic amine 1,3,3-trimethyl-6-azabicyclo[3.2.1]-octane have been used as structure-directing agents for the synthesis of pure silica zeolites in the presence of fluoride. The results are rationalized in terms of the varying size and rigidity of the cations. Both concepts were used in defining a large and rigid spiroammonium derivative which afforded the synthesis of the large pore pure silica zeolite ITQ-7. The existence of structural disorder in ITQ-7, which may be controlled through the water/silica ratio of the synthesis mixture, is confirmed by a number of techniques, but high-resolution electron microscopy results ruled out the existence of stacking faults. Thus, disorder in ITQ-7 does not appear to be due to intergrowths and may correspond to the existence of local defects, probably involving double four ring units, causing lattice strain mainly in the *ab* plane, according to X-ray diffraction simulations.

Introduction

Structure-directing effects during the synthesis of zeolites receive well-deserved attention because of the possibility to synthesize materials with novel structure types amenable to new applications. Thus, efforts to understand why a particular set of synthesis conditions affords the crystallization of a specific zeolite among many other possible structures continue, with the final goal of the a priori design of zeolites for target applications. One of the main structure-directing effects in the synthesis of silica and high silica zeolites is exerted by organic cations that end up occluded within the zeolite void spaces (structure-directing agents, SDA).[1−5] Here we report studies of the structure-directing ability of a series of organic cations with slightly varying size, shape, and conformational flexibility, all derived from the same rigid amine (1,3,3-trimethyl-6-azabicyclo[3.2.1]octane, ABO). The effect of size and flexibility of the cations and of the degree of concentration of the reaction mixtures is discussed. The studies afforded the synthesis of three silica zeolites with novel topologies (structure codes ITE, STF, ISV) and a number of disordered materials. The rationale for the discovery of the large pore silica zeolite ITQ-7 (ISV) is highlighted. We also discuss structural disorder encountered in ITQ-7 materials and how the degree of disorder may be controlled by varying the water/silica ratio in the synthesis mixture.

Experimental Section

Synthesis of the Organic Cations. ABO was used as the parent amine, and different alkyl halides were used for its quaternization (Scheme 1, disregarding enantioisomerism, see below). Methylation and ethylation reactions were carried out in refluxing $CHCl_3$ for

* Corresponding author. E-mail: macamblor@icmm.csic.es.
[†] Universidad Politécnica de Valencia.
[‡] Instituto de Catálisis y Petroleoquímica, Consejo Superior de Investigaciones Científicas.
[§] Praxair, Incorporated.
[||] Georgia Institute of Technology.
[⊥] València Parc Tecnològic.
[⊗] University of Minnesota.
[○] National Institute of Advanced Industrial Science and Technology.
[#] Arrhenius Laboratory.
[▽] Instituto de Ciencia de Materiales de Madrid, Consejo Superior de Investigaciones Científicas.

(1) Gies, H.; Marler, B. *Zeolites* **1992**, *12*, 42.
(2) Gies, H.; Marler, B.; Werthmann, U. *Molecular Sieves*; Springer-Verlag: Berlin, 1998; Vol. 1, p 35.
(3) Davis, M. E.; Lobo, R. F. *Chem. Mater.* **1992**, *4*, 756.
(4) Lobo, R. F.; Zones, S. I.; Davis, M. E. *J. Inclusion Phenom. Mol. Recognit. Chem.* **1995**, *21*, 47.
(5) Kubota, Y.; Helmkamp, M. M.; Zones, S. I.; Davis, M. E. *Microporous Mater.* **1996**, *6*, 213.

10.1021/cm0622248 CCC: $37.00
Published on Web 03/08/2007

Scheme 1. Organocations Used as SDAs in This Work, All Derived from the Central Amine by Quaternization of Its N Atom Using Different Alkyl Halides

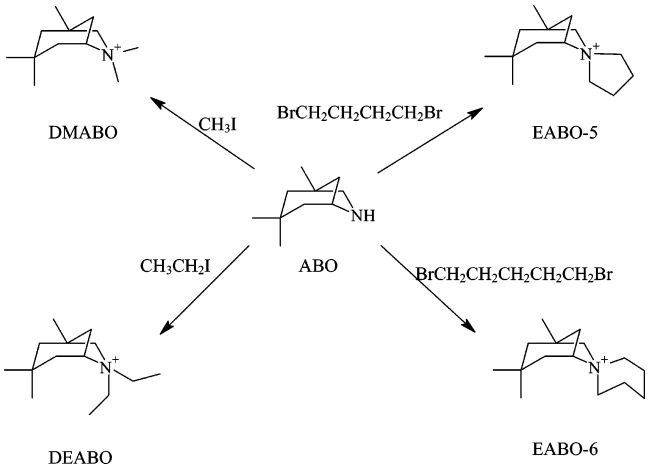

several days using $K_2CO_3 \cdot 1.5H_2O$ as the base, followed by washing with ethyl acetate and final recrystallization in MeOH/ethyl acetate. The preparation of the spiro-cations required a slightly more involved procedure, which is based on an old method to prepare quaternary ammonium salts for the study of Hoffmann degradation processes.[6,7] 1,4-Dibromobutane or 1,5-dibromopentane was added to a NaOH solution and allowed to reflux. Then, the parent amine was added dropwise and allowed to react for 3 h. Addition of a solution of concentrated NaOH precipitates the salt, which is recovered by filtration, washed with diethyl ether, and purified by recrystallization from MeOH/ethyl acetate mixtures. Characterization by ^{1}H NMR and chemical analysis is provided as Supporting Information. The nature of the spirocation synthesized with 1,4-dibromobutane was further confirmed by the structure solution of the corresponding bromide (see below).

Enrichment of the parent amine in one of the enantiomers was carried out by obtaining their solid diastereoisomer salts by using L-tartaric acid in methanol/ethyl acetate mixtures. This procedure was repeated seven times, followed by the measurement of the optical activity in dimethylformamide after each step. The starting racemate was optically inactive, but we observed an increase in activity after each precipitation with L-tartaric acid, confirming that the procedure afforded the enrichment in one enantiomer. However, no plateau was obtained after these cycles, suggesting we have not completely resolved the racemate. After the seventh precipitation the molal optical activity reached a value of +5.7°. Dissolution of the final salt in a basic aqueous solution (pH $\sim$ 12) and the subsequent extraction in $CHCl_3$ gave the enriched amine, which was quaternized to obtain the spiro derivative in the same way as carried out for the racemic mixture.

Structure Determination of EABO-5 ($C_{14}H_{28}BrNO$). M = 306.28, monoclinic, space group $P2_1/c$, a = 8.179(2), b = 14.494(3), c = 26.543(4), β = 97.800(13)°, V = 3117.5(9) Å^3, D_{calcd} = 1.621 g cm^{-3}, λ(Mo Kα) = 0.710 69 Å, T = 293(2) K, μ(Mo Kα) = 3.281 mm^{-1}. Measurements were carried out using a Siemens P4 diffractometer with graphite-monochromated Mo Kα radiation on a colorless crystal of dimensions 0.10 × 0.20 × 0.27 mm. A total of 8687 reflections were collected, of which 4077 were independent (R_{int} = 0.0641). Lorentz, polarization, and absorption (ψ scan, maximum and minimum transmissions 0.299 and 0.167) corrections were applied. The structure was solved by direct methods (SHELXTL) and refined by full-matrix least-squares analysis on F^2. The refinement converged at R1 = 0.058 [$F > 4\sigma(F)$] and wR2 = 0.195 (all data). Largest peak and hole in the final difference map were +0.73 and −0.43 e Å^{-3}. The bromide salt of EABO-5, $C_{14}H_{26}BrN \cdot H_2O$, crystallizes as the true racemic single crystalline phase, and both estereoisomers are depicted in Figure 1, where the closure of a five-ring over N can be seen. Further crystallographic information is provided as Supporting Information.

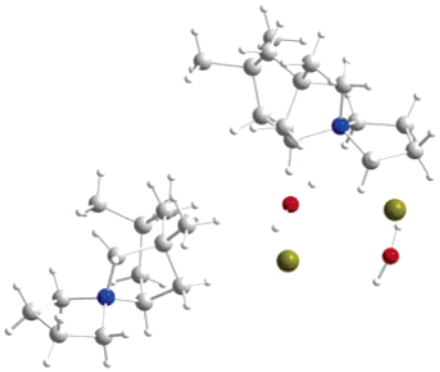

Figure 1. Both enantiomers of EABO-5 as found in $C_{14}H_{28}BrNO$. Two water molecules and two bromide anions are also included. N, blue; O, red; C, gray; H, white; Br, bronze.

Synthesis of Zeolites. The zeolite synthesis followed a well-defined general procedure. Organic cations were used as solutions in their hydroxide form after anion exchange. Tetraethylorthosilicate was hydrolyzed under stirring at room temperature in an aqueous solution of the hydroxide form of the corresponding organic cation. All the ethanol produced plus some water was allowed to evaporate from the gel. The amount of water evaporated was determined by weight, and if necessary, addition of more water allowed the desired water content of the paste to be fixed. Finally, HF (48%) was added while stirring by hand. Preparation of very concentrated gels was accomplished by extensively evaporating water by heating at 80 °C under vacuum after addition of the HF solution. The overall final composition was always 0.5:0.5:1:n ROH/HF/SiO_2/H_2O, where ROH is the hydroxide of the organic cation R^+ and $n \leq 15$. The crystallization was carried out in Teflon lined stainless steel autoclaves which were tumbled at 60 rpm while heated. After heating for a selected time the autoclaves were quenched, and the solids were recovered by filtration and exhaustively washed with deionized water. The products were calcined in ambient air at 580 °C for 3 h.

Characterization. The recovered solids were identified by powder X-ray diffraction (XRD) recorded in a Philips X'Pert or a Philips PW1829 diffractometer (Cu Kα radiation provided by a graphite monochromator). ^{19}F and ^{29}Si magic angle spinning (MAS) NMR spectroscopy of as-made and calcined samples, respectively, was carried out on a Varian VXR 400S WB spectrometer. ^{29}Si MAS NMR spectra of calcined samples were recorded with a spinning rate of 5.5 kHz at a ^{29}Si frequency of 79.459 MHz and a recycle delay of 60 s. The ^{19}F MAS NMR spectra were recorded at a spinning speed of 7.0 kHz, at a frequency of 376.325 MHz with a recycle delay of 5 s. As-made samples were also investigated by ^{29}Si MAS NMR with a $\pi/2$ pulse length of 5 μs and a recycle delay of 60 s and by ^{29}Si{^{1}H} cross-polarization (CP) MAS NMR (contact time 1.5 ms) using a MSL-400 Bruker spectrometer at a frequency of 79.491 MHz. References for chemical shifts were trimethylsilane for ^{29}Si and $CFCl_3$ for ^{19}F.

High-resolution transmission electron microscopy (HRTEM) coupled with selected area electron diffraction (SAED) was used to index the crystal faces and study the possible intergrowths or defects. HRTEM images and SAED patterns were taken with a

(6) Blicke, F. F.; Hotelling, E. B. *J. Am. Chem. Soc.* **1953**, *76*, 5099.
(7) Jewers, K.; McKenna, J. *J. Chem. Soc.* **1958**, 2209.

JEOL ARM 1250 microscope operating at 1250kV (Cs = 1.7 mm). The images were obtained after the samples were crushed, dispersed in acetone, and placed on a holey carbon microgrid.

Disorder Simulations. The XRD patterns of ITQ-7 were calculated using the Reflex module of Materials Studio (Accelrys, Inc.). Lattice strain broadening effects (0−2%) were included in the calculations, according to the established theory.[8] A pseudo-Voigt[8,9] profile was adopted. Because these simulations were focused upon explaining the structural disorder, we used only minimal instrumental broadening[9] parameters ($U = V = W = 0.01$) with a Lorentzian−Gaussian mixing parameter $\eta = 0.5$.

Results and Discussion

Strategies in the Design of SDA Cations. Although zeolite synthesis is still largely based on trial and error, the empirical knowledge derived over the last few decades, especially from the works of Gies, Davis, Zones, and their respective co-workers, allows synthesis strategies for the discovery of new zeolites to be conceived.[1] For this "directed trial and error approach", the first step is to realize that silica frameworks themselves do not vary much in their relative stabilities[10] and that crystallization kinetics is of large importance and depends on a number of factors that are convenient to screen.[11] Second, the interaction between the inorganic framework and the organic SDA may help to stabilize a given zeolite.[12] And even if the stabilization energy is not large,[13] if the SDA is to be occluded in the final material, the size and shape of an SDA may prevent the crystallization of some zeolites while allowing others with larger or more appropriately shaped voids to form. This allows for some rational design of organic cations to be used as SDAs. However, the rigidity of the organic cation needs also to be considered as a very important feature determining its structure-directing ability: a highly flexible cation with multiple possible conformations may more easily adapt to the channels of different zeolites, giving it a low specificity in structure direction and a greater chance of yielding a zeolite that easily nucleates and grows (i.e., the so-called "default zeolites", such as, for instance, the medium pore ZSM-23 zeolite, which crystallized when linear diquats of varying length were unable to produce an ideal fit inside other frameworks).[14] Thus, in the search for new structures the use of rigid SDA cations may represent a meaningful strategy. Also, an SDA with a featureless shape (such as a globular cation that can fit in different void spaces) may be expected to show a lower specificity than a more distinctly shaped cation of similar size.

In our work to make new large pore zeolites, we based our strategy on the points above and paid particular attention to the rigidity and molecular shape aspects that directed our choice of SDA cations. To this end, we synthesized five different cations derived from the rigid polycyclic ABO (Scheme 1). The parent amine, which is no longer commercially available, shows a large conformational rigidity and a relatively big size, with a nonglobular and a nonlinear shape. It also contains two asymmetric centers, and the commercial product did not show any optical activity, actually being a racemic mixture of two (R,S) and (S,R) enantiomers (the methylene bridge preventing the existence of the (R,R) and (S,S) enantiomers). A chiral, enantiomerically pure SDA could eventually be used to synthesize a chiral, enantiomerically pure zeolite, if a good geometric fit between the cation and the zeolite void space was achieved. In the following, the SDA derived from the ABO amine will correspond to a racemic mixture, unless otherwise noted.

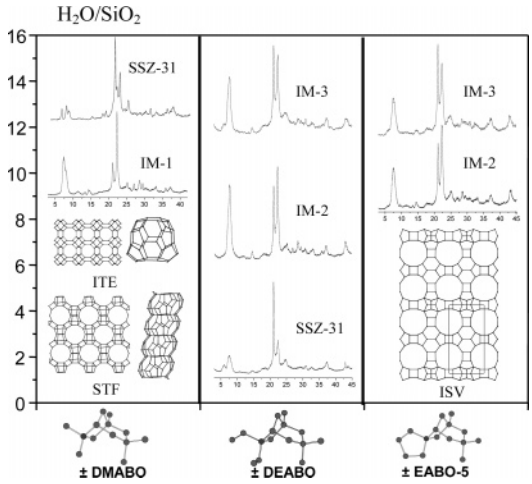

Figure 2. Summary of synthesis results for DMABO, DEABO, and EABO-5.

The SDAs we derived from ABO (Scheme 1) are the dimethyl cation (DMABO), the diethyl cation (DEABO), the spirocation formed by quaternization of the N atom through a chain of four methylene groups to yield a new five-membered ring cycle (EABO-5), the same cation enriched in the dextro form ((+)EABO-5) by successive recrystallizations of the L-tartrate salt, and the spirocation with a new six-membered cycle around N (EABO-6). The conformational freedom of the SDAs increases in the order DMABO < EABO-5 < EABO-6 < DEABO, and their size increases in the order DMABO < EABO-5 < DEABO < EABO-6.

As we have shown previously for other SDA cations,[15] the water to silica ratio significantly determines the phase selectivity of the crystallization of silica phases in aqueous fluoride media, and it is, thus, one of the important parameters to be systematically tested. Typically, a large dilution favors the formation of dense phases (tridymite-like solids), while decreasing the water/silica ratio is frequently needed to afford materials with a lower framework density. This is an empirical trend observed by us in the synthesis of silica zeolites using quaternary ammonium cations in fluoride media and[15,16] later corroborated by Zones and co-workers.[17]

(8) Young, R. A. *The Rietveld Method*; IUCr Monographies of Crystallography 5; Oxford University Press: Oxford, 1993.
(9) Caglioti, G.; Paoletti, A. B.; Ricci, F. P. *Nucl. Instrum. Methods* **1958**, *3*, 223.
(10) Piccione, P. M.; Laberty, Ch.; Yang, S.; Camblor, M. A.; Navrotsky, A.; Davis, M. E. *J. Phys. Chem. B* **2000**, *104*, 10001.
(11) Davis, M. E.; Zones, S. I. In *Synthesis of Porous Materials. Zeolites, Clays and Nanostructures*; Occelli, M. L., Kessler, H., Eds.; Marcel Dekker, Inc.: New York, 1997; p 1.
(12) Burton, A.; Lee, G. S.; Zones, S. I. *Microporous Mesoporous Mater.* **2006**, *90*, 129.
(13) Piccione, P. M.; Yang, S.; Navrotsky, A.; Davis, M. E. *J. Phys. Chem. B* **2002**, *106*, 3629.
(14) Moini, A.; Schmitt, K. D.; Valyocsik, E. W.; Polomski, R. F. *Zeolites* **1994**, *14*, 504.
(15) Camblor, M. A.; Villaescusa, L. A.; Díaz-Cabañas, M. J. *Top. Catal.* **1999**, *9*, 59.
(16) Villaescusa, L. A. Ph.D. Thesis, Universitat Politècnica de Valencia, 1999.

Table 1. Summary of the Experiments Carried Out in the Synthesis of Zeolites Using EABO-5 as the SDA

experiment	H_2O/Si	*T* (°C)	*t* (days)	pH	*R* (%)	product
L488	15	150	17	7.5	12.9	amorphous
			27	7.6	14.2	amorphous
			38	8.0	15.8	MI-3
L532	12.5	150	19	8.2	14.5	amorphous
			35	8.3	13.8	MI-2 + ITQ-7 (<5%)
			61	8.7	14.4	MI-2
L522	10	135	21	7.8	14.9	amorphous
			42	7.8	16.3	Dmax-ITQ-7
			56	8.2	14.5	Dmax-ITQ-7
L503	10	150	16	7.8	18.4	Dmax-ITQ-7
			16	7.6	18.6	Dmax-ITQ-7
L504	10	175	16	7.0	14.5	tridymite
			16	6.5	15.4	Tridymite
L473	7.5	150	13	8.2	20.5	Dmax-ITQ-7
			21	7.9	21.6	Dmax-ITQ-7
L474	7.5	175	4	7.6	19.0	amorphous
L502	7.5	175	16	7.0	17.5	MI-2 (∼50%) + ITQ-7 (<5%)
L501	5	175	10	7.0	21.4	ITQ-7 (∼50%) + MI-2 (<5%)
L489	5	150	10	7.9	24.4	Dmed-ITQ-7 + β (<5%)
			20	7.6	23.8	Dmed-ITQ-7 + β (<5%)
L491	2-3	135	14	8.8	27.8	β + ITQ-7 (<5%)
L492	2−3	150	7	8.2	27.8	Dmed-ITQ-7 + β (<5%)
L493	2−3	175	5	7.2	24.9	Dmed-ITQ-7 (∼80%)
L497	2−3	175	6	6.9	25.7	Dmed-ITQ-7 (∼80%)
			12	6.9	26.9	Dmed-ITQ-7
L508	2−3	165	7	7.5	28.7	Dmed-ITQ-7
			15	7.0	25.4	Dmed-ITQ-7
			25	7.1	26.9	Dmed-ITQ-7
L509	<1	175	7	7.1	31.1	amorphous
			15	6.3	30.3	ITQ-7 (∼10%)
			30	5.9	30.2	ITQ-7 (∼90%)
L535	<1	175	25	7.4	25.4	MNI-13 < 5%
			34	7.6	26.6	ITQ-7 < 5%
			53	6.4	27.1	tridymite + ITQ-7
L536	<1	150	55	6.3	29.5	Dmin-ITQ-7
L546[a]	<1	175	15	8.2	34.8	Dmin-ITQ-7
L547[a]	<1	150	15	7.7	34.5	Dmin-ITQ-7

[a] Synthesis with seeds (as-made Dmed-ITQ-7, 5 wt % of silica in ITQ-7 over silica in the gel).

Table 2. Synthesis Results Using EABO-6

experiment	H_2O/Si	*T* (°C)	*t* (days)	pH	*R* (%)	product
EP308	7.5	150	13	7.54	18.05	ITQ-7 + Beta
			31	7.35	19.1	ITQ-7 + Beta
EP309	5	150	13	6.85	14.2	Dmed-ITQ-7
EP306AC	2.5	150	7	7.22	24.17	Beta
			14	7.10	24.11	Beta
EP306D	2.5	135	14	8.00	21.20	Beta
EP306B	2.5	175	7	6.17	20.56	Beta + ITQ-7

A similar trend was first noticed by Gies and Marler in the synthesis of chlathrasils using amines in alkaline conditions.[1] Thus, we have restricted our search to water to silica ratios equal to or smaller than 16. Figure 2 shows a summary of the synthesis results using DMABO, DEABO, and EABO-5. More complete information is given below for EABO-5 (Table 1) and in the Supporting Information for DMABO and DEABO (Tables 1S and 2S). At the high water content side, severely intergrown structures likely related to Beta and SSZ-31 crystallize. For the more flexible cation, DEABO, this also occurs at more concentrated conditions. We note that, in the synthesis conditions employed here, zeolite Beta should be considered as a "default structure", especially at concentrated conditions, meaning that no specific structure direction by the cation is needed: no less than 17 organic cations, very different in size, shape, rigidity, and C/N ratios, have been used to produce silica Beta or Beta-like materials.[18] The predominance of Beta and related intergrown structures when using DEABO may be postulated to be a consequence of the conformational flexibility of the ethyl chains of this cation.

Several interesting structures appear at more concentrated conditions when using the more rigid DMABO and EABO-5 cations. DMABO has afforded the synthesis of the pure silica zeolites ITQ-3 (ITE, 2D, 8MR)[19] and ITQ-9 (STF, 1D, 10MR),[20] both presenting cages large enough to accommodate the large SDA. The EABO-5 cation was synthesized considering that, being larger than DMABO, it could prevent the crystallization of ITE and STF, while its large conformational rigidity was expected to increase the degree of specificity in its structure-direction ability compared to DEABO. EABO-5 afforded the synthesis of ITQ-7,[21] which at the time of its discovery was the pure SiO_2 crystalline material with the lowest framework density and the second high silica zeolite, after Beta, to possess a three-dimensional (3D) system of large pore channels. ITQ-7 possesses a 3D

(17) Zones, S. I.; Darton, R. J.; Morris, R.; Hwang, S. J. *J. Phys. Chem. B* **2005**, *109*, 652.

(18) Camblor, M. A.; Barrett, P. A.; Díaz-Cabañas, M. J.; Villaescusa, L. A.; Puche, M.; Boix, T.; Pérez, E.; Koller, H. *Microporous Mesoporous Mater.* **2001**, *48*, 11.

(19) Camblor, M. A.; Corma, A.; Lightfoot, P.; Villaescusa, L. A.; Wright, P. A. *Angew. Chem., Int. Ed.* **1997**, *36*, 2659.

(20) Villaescusa, L. A.; Barrett, P. A.; Camblor, M. A. *Chem. Commun.* **1998**, 2329.

(21) Villaescusa, L. A.; Barrett, P. A.; Camblor, M. A. *Angew. Chem., Int. Ed.* **1999**, *38*, 1997.

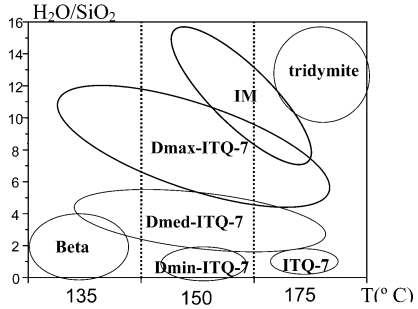

Figure 3. Product distribution diagram using EABO-5 as the SDA, as a function of the water content and temperature.

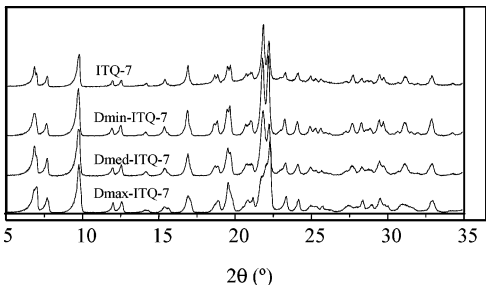

Figure 4. Powder XRD patterns of as-made ITQ-7 materials. The materials are classified according to their increasing degree of disorder (from top to bottom).

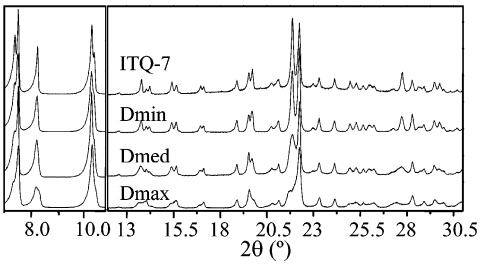

Figure 5. Powder XRD patterns of calcined ITQ-7 materials with different degrees of disorder. Note that the intensity of the low angle range has been divided by ~1.8 for the sake of clarity.

system of large pore channels open through 12-membered rings (ISV, 3D, 12MR).

The difference in selectivity of DMABO and EABO-5 may be thus ascribed to the larger size of the latter preventing the formation of ITE or STF. With regard to DEABO and EABO-5, one can formally go from one to the other by simply joining the end of the ethyl groups to make a four methylene chain, so the difference between both cations is, essentially, a slightly smaller size plus a significant decrease in conformational freedom at one end of the molecule for EABO-5 compared to DEABO. It is indeed interesting and instructive to realize that such a relatively small change imparts a large difference in the structure-direction properties of both cations (ITQ-7 was never detected when using DEABO). In order to test this idea, we have also synthesized EABO-6, with a slightly larger size and a slightly higher conformational freedom than EABO-5, and compared the structure-direction ability of both cations. As shown in Table 2, EABO-6 is also able to produce ITQ-7 but with a lower specificity and a greater tendency to produce the default structure (zeolite Beta), as expected due to its larger conformational freedom. This is in contrast to the results

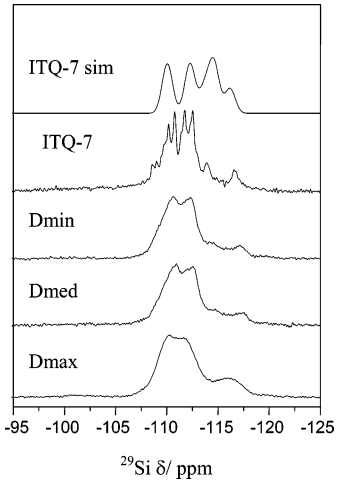

Figure 6. ^{29}Si MAS NMR spectra of calcined ITQ-7 materials with varying degrees of order (as observed by powder XRD). The upper trace is a simulation obtained using the average Si−O−Si angles and the equation of Thomas et al.[27]

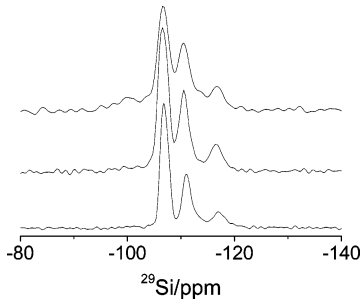

Figure 7. ^{29}Si{^{1}H} CP MAS NMR (1.5 ms contact time) spectra of as-made ITQ-7 disordered materials. From top to bottom: Dmin, Dmed, and Dmax (as observed by powder XRD). Bloch decay spectra and deconvolution of CP and Bloch decay spectra are available as Supporting Information.

recently reported by Song et al. also using EABO-6,[22] where they conclude a higher specificity of EABO-6 toward ordered ITQ-7 (see below).

We will now focus on ITQ-7, a silica zeolite which is interesting because of its low framework density, its interconnected system of large pores, its structural relationship to the zeolite Beta family, and the structure-direction effects affording its synthesis.

Synthesis of Zeolite ITQ-7. Table 1 lists the synthesis results using EABO-5 at different conditions. The main parameter screened was the water to silica ratio and the crystallization time at 150 °C. In Table 1 there are several codes which need to be explained. The codes Dmin, Dmed, and Dmax preceding the name ITQ-7 refer to ITQ-7 materials with distinct degrees of order (minimum, medium, and maximum, respectively) as explained below, with the utmost ordered material referred to just as ITQ-7. MI-2 and MI-3 denote two distinct intergrown materials likely related to the Beta and SSZ-31 families, in view of their XRD patterns (see Supporting Information, Figure 1S).[23] The crystallization of these intergrown materials is favored at higher temperature and higher water content, and beyond their crystallization field (higher temperature at medium dilution) tridymite also

(22) Song, J. Q.; Marler, B.; Gies, H. *C. R. Chim.* **2005**, *8*, 341−352.
(23) Lobo, R. F.; Tsapatsis, M.; Freyhardt, C. C.; Chan, I.; Chen, C. Y.; Zones, S. I.; Davis, M. E. *J. Am. Chem. Soc.* **1997**, *119*, 3732.

Table 3. Relative Intensities of the Deconvoluted ^{29}Si MAS NMR Resonances of As-Made ITQ-7 Materials with Varying Degrees of Order

L546C (Dmin)		L508 (Dmed)		L522B (Dmax)	
center	% area	center	% area	center	% area
−117.2	18.0	−116.6	12.8	−116.9	10.1
−114.0	5.2	−113.2	3.6	−113.5	8.4
−111.1	35.1	−110.6	31.9	−110.5	26.5
−107.2	41.8	−106.6	49.3	−106.7	46.9
		−102.0	2.4	−100.1	8.1

crystallizes, as shown graphically in Figure 3. For the ITQ-7 materials, the degree of order generally increases when the water to silica ratio decreases, although at the lowest temperature tried (135 °C), the most concentrated conditions yield zeolite Beta. We have to note also that for very small water contents ($H_2O/SiO_2 < 1$) some uncertainty occurs: in experiments L509 and L535 the water to silica ratio is smaller than 1 and difficult to determine accurately, and both experiments yielded quite different results. In addition to the uncertainty in the H_2O/SiO_2 ratio, the reasons for the dissimilar results may be due to the relatively harsh treatments required to achieve those low ratios (see Experimental Section). By using seeds under similar synthesis conditions, it is possible, however, to speed up the crystallization and to ensure the formation of ITQ-7 (last entries in Table 1).

Figure 4 shows representative XRD patterns of different types of as-made pure silica ITQ-7 materials. It can be observed that there are certain reflections which vary in width and position, although the differences are relatively subtle. After calcination (Figure 5), the differences become more noticeable, perhaps as a result of a general narrowing of the reflections compared to the as-made samples. For instance, in the 2θ range 21−23°, the peak at around 22.2° is narrow and roughly invariant among samples, but at lower angles some samples show a narrow peak at around 21.8° that in other samples becomes wider and apparently shifts to a lower angle. The different patterns suggest different degrees of structural order in materials with the reported ISV structure. These differences are consistent throughout the patterns and allow us to classify on a qualitative basis four types of ITQ-7 zeolites with increasing amounts of disorder using the XRD patterns of the calcined materials (see Table 1): ITQ-7 (ordered), Dmin-ITQ-7, Dmed-ITQ-7, and Dmax-ITQ-7.

It is interesting that, from over 30 samples of ITQ-7 prepared, all of them belong to one or another of the four categories. From Table 1, we can conclude that the degree of order can be controlled by just varying the synthesis conditions, particularly the dilution of the synthesis mixture. In a different system, it has been shown that temperature and concentration are the key factors in controlling stacking faults in pure silica zeolite SFF/STF intergrowths prepared in fluoride media.[24] In our case, at 150 °C the degree of order clearly increases as the water to silica ratio decreases (Figure 3). The water/SiO_2 ratio appears to determine the degree of order even when ITQ-7 with a different degree of order is used as seeds (Table 1, last entries: seeding with Dmed at low water/SiO_2 ratios produces Dmin). This suggests nucleation is not critical to the degree of disorder. Quite surprisingly, when EABO-5 (Table 1) and EABO-6 (Table 2) are used under otherwise identical conditions, the ITQ-7 materials obtained show approximately the same degree of order, although EABO-6 shows a greater tendency to produce zeolite Beta (Tables 1 and 2) at variance with the conclusions drawn by Song et al., who concluded a better specificity of EABO-6 toward ordered ITQ-7.[22] This apparent discrepancy may be due first to the fact that Song et al. compared their results with our previous report,[21] which only contained a limited range of experimental results, and second to the greater attention that Song et al. devoted to the as-made ITQ-7 materials compared to the calcined ones. In our view, structural disorder in ITQ-7 is more evident in the XRD patterns of calcined (Figure 5) than of as-made materials (Figure 4). Regardless, currently available experimental data do not allow any definitive conclusions regarding the specificity in structure direction of both cations.

Structural Disorder in ITQ-7. In addition to the XRD features described above, disorder in ITQ-7 has been confirmed by ^{29}Si MAS NMR of the calcined samples. As shown in Figure 6, the sharp resonances found in the spectrum of the most ordered ITQ-7 material that we have synthesized become increasingly broadened for the so-called Dmin, Dmed, and Dmax-ITQ-7. This broadening is remarkable because for calcined SiO_2 materials prepared by the fluoride route the absence of both heteroatoms and Si−OH defects typically yield spectra with narrow resonances.[25,15] We ascribe that broadening to structural disorder. Similarly, the ^{29}Si MAS NMR spectra of pure silica zeolite Beta samples vary considerably depending on synthesis conditions: some samples show sharp resonances and a relatively good resolution, while some present broad and overlapped resonances, which has been attributed to the different sizes of the domains of pure polymorphs (or, in other words, to the frequency of stacking faults).[26] Note also that a small concentration of Q3 is observed in the most disordered ITQ-7 samples (Dmax). Also note that the spectrum of Dmin-ITQ-7 is already very different from that of ordered ITQ-7, despite the minor differences in the XRD patterns of both types of samples.

Interestingly, all of the four experimental spectra are markedly different from that simulated using the equation of Thomas et al.[27] and the Si−O−Si angles of the reported structure (Figure 6), suggesting further structural work is still needed even for the most ordered material. Furthermore, when considering that the ordered sample contains more sites than reported in space group $P4_2/mmc$ (three sites with a multiplicity of 16 and two sites with a multiplicity of 8) the symmetry of the ordered phase should be lower than reported. In agreement with the results by Song et al., our attempts to refine the structure in several subgroups of $P4_2/mmc$ against synchrotron data proved unsuccessful, possibly as a result of the large number of structural parameters. There were no

(24) Villaescusa, L. A.; Zhou, W.; Morris, R. E.; Barrett, P. A. *J. Mater. Chem.* **2004**, *14*, 1982.
(25) Chézeau, J. M.; Delmotte, L.; Guth, J. L.; Soulard, M. *Zeolites* **1989**, *9*, 78.
(26) Valencia, S. Ph.D. Thesis, Universitat Politècnica de Valencia, 1997.
(27) Thomas, J. M.; Klinowski, J.; Ramdas, S.; Hunter, B. K.; Tennakoon, D. T. B. *Chem. Phys. Lett.* **1983**, *102*, 158.

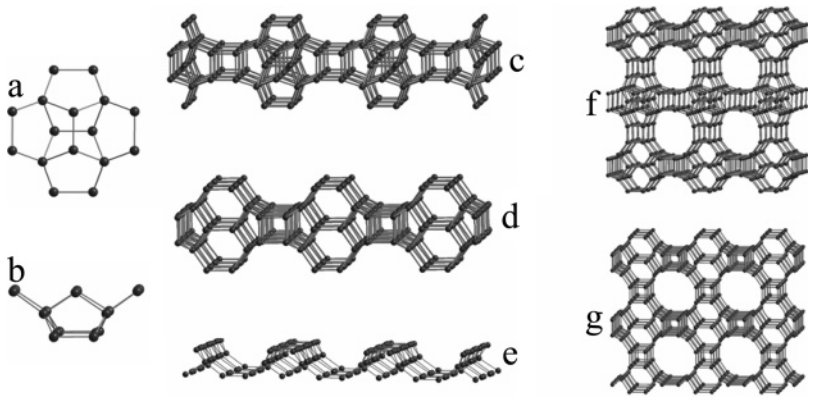

Figure 8. Structural relationship between polymorph C of Beta (BEC) and ITQ-7 (ISV). A secondary building unit composed of 16 T atoms (a and b, from two different viewing points) may be used to build the periodical building unit (PerBU, c and d) found in polymorph C (BEC) of the Beta family and in ISV. In both structures adjacent PerBU layers are joined without translation through D4R. When the PerBU is not rotated, polymorph C (g) is formed, while a 90° rotation of alternate layers produces ISV. Polymorph C may also be described by using the PerBU depicted in e, which is also the PerBU of polymorphs A and B of the Beta family.

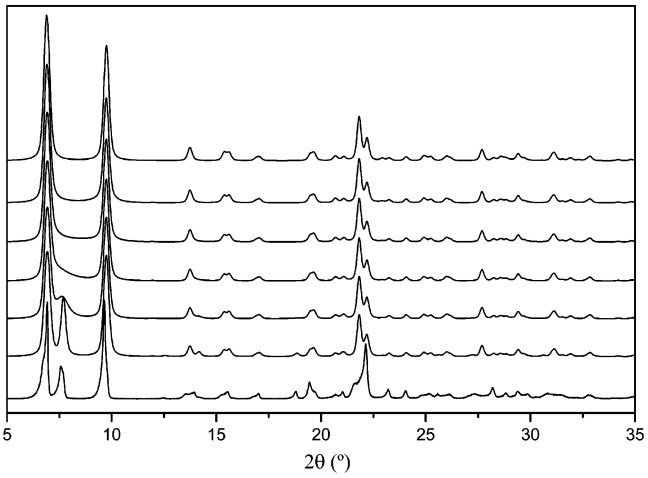

Figure 9. XRD patterns of ISV/BEC intergrowths simulated using DIFFaX (from bottom to top the ISV stacking probability is 99, 80, 60, 40, 20, and 1%). The lower-most trace is the experimental pattern of a material with maximum degree of XRD disorder (Dmax).

hints of symmetry lowering in the synchrotron diffraction patterns of ordered ITQ-7.[21]

The existence of connectivity defects in the calcined samples (Figure 6) prompted us to investigate the as-made samples by ^{29}Si MAS NMR and CP MAS NMR, in which no annealing of defects by postsynthesis heating may occur. There appears to be a correlation between the degree of structural disorder and the relative intensity of the Q3 resonance in both the ^{29}Si CP MAS NMR spectra of the as-made samples (Figure 7) and the ^{29}Si MAS NMR (Supporting Information, Figure 2S). Additionally, the disordered samples show broader resonances. Table 3 lists the results of a deconvolution of each ^{29}Si MAS NMR spectrum, showing that the concentration of connectivity defects in the as-made samples slightly increases as the degree of disorder increases. Thus, for Dmin samples the concentration of defects is negligible, while it is relatively large for Dmax samples, where up to 5 Si atoms out of 64 per unit cell are Q3 sites.

ITQ-7 is clearly related to zeolite Beta (see below), a typical example of an intergrown zeolite, which shows extensive stacking faults yielding an XRD patterns with broad and sharp reflections.[28] Unlike the zeolite Beta case,[28] we have been unable to find a law for the sharp and broad XRD reflections of ITQ-7 based on their Miller indices. Despite this and given the structural relation between ISV and the Beta family, the patterns shown in Figures 4 and 5 suggested to us the existence of stacking faults in ITQ-7 (a list of invariant and variant reflections in ITQ-7 is given as Supporting Information, Table 3S).

The structural relationship between ISV and the Beta family may be described on the basis of the tertiary building unit highlighted in Figure 8, which contains 16 silicon atoms, the "T16 unit".[29] In the Beta family, a basic periodical building unit (PerBU) is constructed by translations of T16 along *a* and *b*. This PerBU may be connected, after a rotation of 90° along [001], to the next PerBU in three different ways: without shift, with a shift of $^1/_3a$ or $^1/_3b$ or with a shift of $-^1/_3a$ or $-^1/_3b$. When no shift is applied, polymorph C (BEC) is formed. In ISV, the tertiary building unit is the same T16, and the PerBU may be conveniently chosen to be a double layer constructed by linking together, without lateral shifts and with a 90° rotation normal to the plane of the layer, the Beta PerBU. If these "double layers" are then linked together without rotation, polymorph C (BEC) is also built, while if the double layers are rotated by 90° normal to the plane of the layer, ISV is obtained (see ref 29 for details and ref 22 for a different description). The symmetry of both BEC and ISV is $P4_2/mmc$, although the direction of the fourfold axis relative to the above referenced layers is different in both topologies, and in ISV there is a doubling of the cell along [001].[21] In both polymorphs there are double four-member rings (D4R): inside the PerBU layer, adjacent double T16 units are linked through D4R, while each PerBU is linked to the next one again through D4R. However, while in BEC all the D4R units are equivalent by symmetry, in ISV there are two types of crystallographically distinct D4R, centered at special positions 2a and 2f, respectively, in space group $P4_2/mmc$.

(28) Newsam, J. M.; Treacy, M. M. J.; Koetsier, W. T.; de Gruyter, C. B. *Proc. R. Soc. London, Ser. A* **1988**, *420*, 375.
(29) Gies, H.; van Koningsveld, H. Catalog of Disorder in Zeolite Frameworks. http://www.iza-structure.org/databases/ (accessed May 2006) (published on behalf of the Structure Commission of the International Zeolite Association).

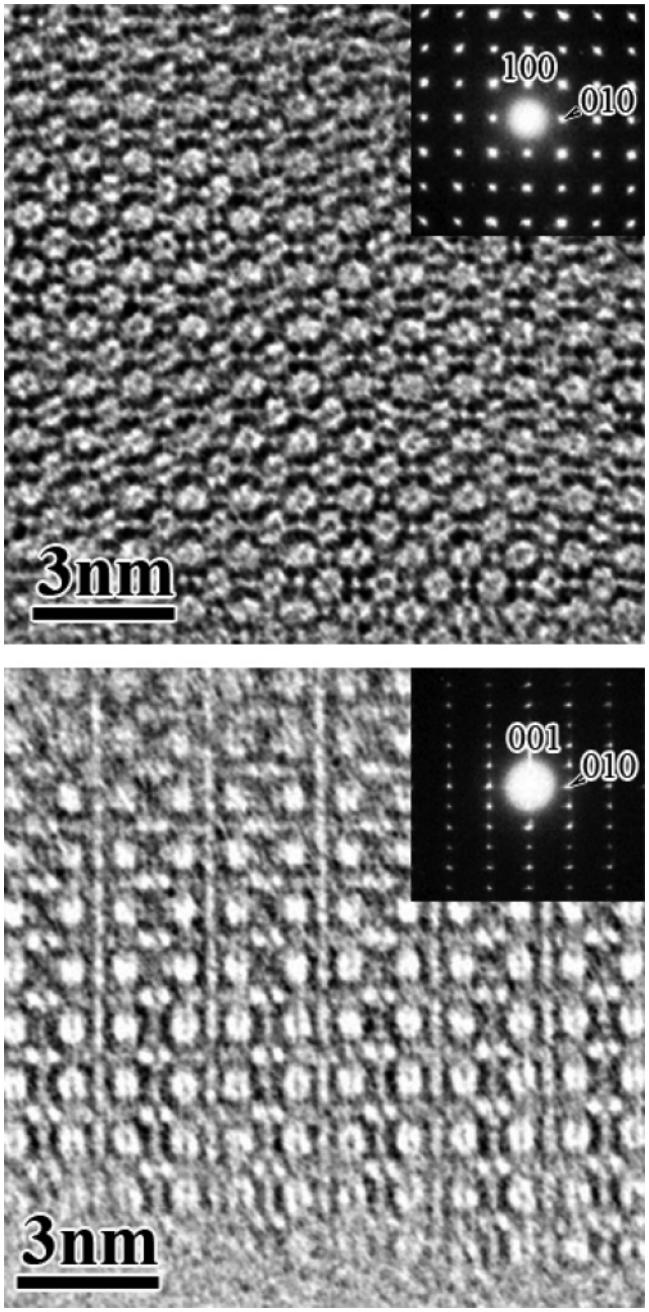

Figure 10. HRTEM images and the corresponding ED patterns (insets) of an ITQ-7 material with maximum degree of XRD disorder (L473). Crystal projections can be indexed as [001] (top) and [100] (bottom) of highly crystalline ITQ-7 (ISV).

This close structural relationship raised the possibility that the structural disorder in ITQ-7 might be due to stacking faults and, particularly, to intergrowths between ISV and the polymorphs of the Beta family. A particularly obvious candidate for intergrowing with ISV is the BEC topology, polymorph C, because of their similar tetragonal arrangements of D4R, which allows a perfect matching of the respective layers. This allows models for stacking faults in one direction that would depend on the existence or absence of a 90° rotation in every other PerBU "double layer" described above. A convenient way to simulate the diffraction patterns of such an intergrowth is by using DIFFaX,[30] and the results are depicted and compared to ITQ-7 materials in Figure 9. As recently reported by Song et al.,[22] powder XRD

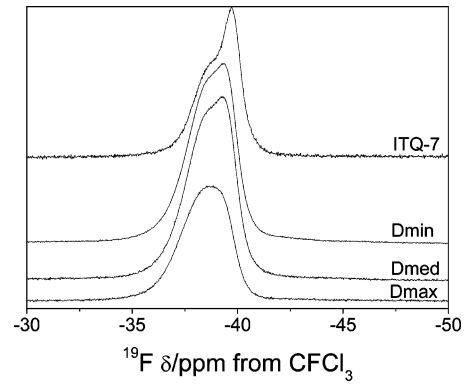

Figure 11. ^{19}F MAS NMR spectra of as-made ITQ-7 materials with varying degrees of order (as observed by powder XRD).

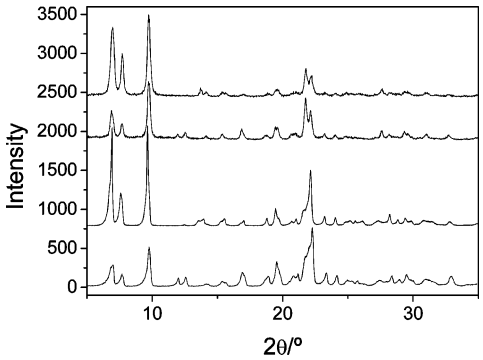

Figure 12. Powder XRD patterns of as-made and calcined ITQ-7 materials obtained under similar synthesis conditions ($H_2O/SiO_2 = 7.5$, 150 °C) but with or without Ge. From bottom to top, as-made and calcined pure SiO_2 ITQ-7 and as-made and calcined Ge-ITQ-7 (Si/Ge = 5).

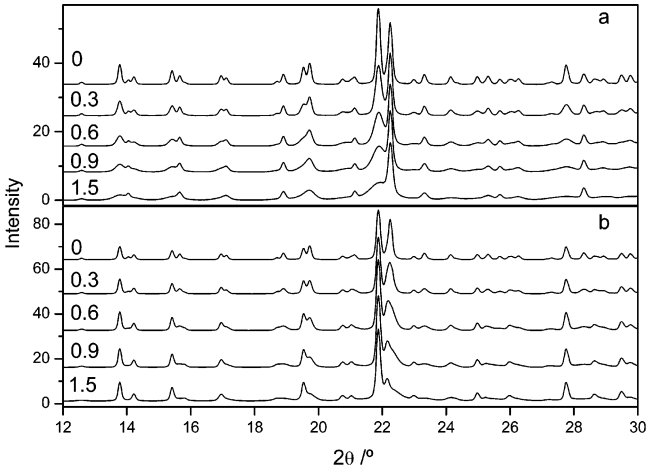

Figure 13. Simulated XRD patterns of ITQ-7 with lattice strain in the *ab* plane (a) or along *c* (b). Percentage of lattice strain is given close to each trace.

diffraction is not very sensitive to BEC/ISV intergrowths for intermediate probabilities of stacking faults, which led those authors to speculate that disordered ISV/BEC intergrown materials have been already synthesized, although not being recognized as such intergrowths. Comparison of ITQ-7 XRD patterns and ISV/BEC simulations (Figure 9) allows us to rule out the presence of BEC domains in amounts greater than 10−20%. With regard to our disordered materials, the BEC/ISV simulation clearly fails to account for the

(30) Treacy, M. M. J.; Deem, M. W.; Newsam, J. M. *DIFFaX*, version 1.801; 1995; Treacy, M. M. J.; Newsam, J. M.; Deem, M. W. *Proc. R. Soc. London A* **1991**, *433*, 499.

Table 4. Synthesis Results Using EABO-5 Enriched in the Dextrorotary Isomer

experiment	*T* (°C)	H_2O/Si	*t* (days)	pH	*R* (%)	product
L542	135	2−3	14	9.4	29.3	Beta (∼75%) + ITQ−7 (∼25%)
			27	7.9	28.7	Beta (∼75%) + ITQ−7 (∼25%)
L543	150	2−3	11	7.6	27.8	Dmed-ITQ-7 + Beta (<5%)
			25	7.23	27.4	ITQ-7 + Beta (<5%)
L544	175	2−3	11	6.9	22.3	Dmed-ITQ-7
			18	7.6	27	Dmed-ITQ-7
L545	150	10	18	8.0	17.1	MI-3 + ITQ-7 (<5%)
L549	120	2−3	28	9.4	29.1	Beta + ITQ-7 (<10%)
L550	100	2−3	48	9.8	29.9	amorphous (<80%) + ITQ-7 + Beta

changes observed in the diffraction patterns of ITQ-7 materials.

We have worked with plastic and virtual models trying to find other possible arrangements of stacking faults in ITQ-7 without success. Apart from BEC, other polymorphs of the Beta family cannot intergrow with ISV in an obvious way and, certainly, not by stacking faults in a single direction. Thus, we looked for additional information by examining ITQ-7 disordered materials by HRTEM and electron diffraction (ED). Transmission electron microscopy (TEM) images coupled with SAED patterns were used to identify the ITQ-7 symmetry, space group $P4_2/mmc$. Sample L473, which has an XRD pattern displaying maximum disorder (Dmax), has been exhaustively studied by ED finding no streaking or extra spots due to possible intergrowths or stacking faults. Mixtures of phases were also rejected by ED, every diffraction pattern being indexed as $P4_2/mmc$. Besides that, tilting the crystals along the main zone axis with the electron beam parallel to the *a*-, and *c*-axes shows visual differences with polymorph C of zeolite beta. Figure 10 shows HRTEM images and the corresponding SAED patterns of the [100] and [001] projections of L473 crystals. Thus, we have to conclude that the observed disorder in ITQ-7 materials is not due to stacking faults. This is stronger evidence than the DIFFaX results (Figure 9), favoring the absence of ISV/BEC intergrowths in ITQ-7, and detracting from the aforementioned conjecture stating that such intergrown materials might have been prepared but not identified.[22]

We consider this as an important finding because, given the similarities between BEC and ISV, intergrowths of both topologies could have been anticipated, in agreement with the expectations by Song et al.[22] Actually, pure silica materials with the BEC topology have a real existence as overgrowths on "standard" Beta crystals,[31] a result that may point to BEC crystals having more difficulty in nucleating than in growing, under the synthesis conditions described in ref 31. Also, the existence of D4R in pure silica "standard" Beta materials synthesized by the fluoride route with several different SDAs has been well established by ^{19}F MAS NMR, implying the existence in Beta of polymorphs different from A and B, which completely lack D4R.[18] Furthermore, lattice energy minimization calculations suggest SiO_2 materials with the BEC topology are slightly more stable than those with the ISV topology (see Supporting Information, Table 4S). The definitive lack of stacking faults in ITQ-7 suggests that EABO-5 and EABO-6 show a certain specificity toward ISV, or perhaps it is more appropriate to say that they show a certain specificity *against* BEC, thus precluding the formation of BEC domains.

The lack of stacking faults in disordered ITQ-7 materials and, in fact, the lack of any obvious sign of disorder by ED and HRTEM forced us to look at other characterization techniques that probe shorter distances, such as NMR. The ^{29}Si MAS NMR results have been described above, and while apparently confirming the existence of disorder, do not yield further information on its nature apart from the very small increase in defect concentrations as the disorder increases. The ^{19}F MAS NMR spectra are depicted in Figure 11. For the most ordered material, two overlapping resonances at −38.5 and −39.3 ppm can be unambiguously ascribed to fluoride occluded in D4R units,[32,18] each one corresponding to two different crystallographic sites (internal to the "double layer" PerBU and in between successive PerBU, without specific assignments at this time to which resonance corresponds to each site). As the degree of XRD disorder increases, the signal at higher field becomes broader and both merge into an asymmetrical resonance for the more disordered samples (Figure 11). Attempts to deconvolute the spectra into two mixed Lorentzian−Gaussian lines only succeeded in the ordered ITQ-7 (4:6 intensity ratio for the high and low field resonances, respectively, close to the 1:1 theoretical ratio) but visual inspection of the spectra suggests an increased relative intensity of the downfield signal for the disordered samples. The absence of resonances other than those around −40 ppm indicates that F is occluded only in D4R cages and not in other cages found in zeolite Beta. This again suggests the absence of polymorphs A and B of the Beta family, which typically exhibit additional resonances in the −58 to − 70 ppm range.[18]

The NMR results all support the existence of varying degrees of disorder in ITQ-7 materials and give some additional information:

(i) ^{29}Si MAS NMR and ^{29}Si CP MAS NMR on the as-made samples demonstrate that, as the degree of XRD disorder increases, the concentration of connectivity defects increases, though only very slightly.

(ii) ^{29}Si MAS NMR on the calcined samples also agree with the above, although less conclusively because of the possibility of defect annealing effects.

(iii) Finally, in the ^{19}F MAS NMR spectra of the as-made samples the resolution of resonances decreases as the degree

(31) Liu, Z.; Ohsuna, T.; Terasaki, O.; Camblor, M. A.; Díaz-Cabañas, M. J.; Hiraga, K. *J. Am. Chem. Soc.* **2001**, *123*, 5370.

(32) Caullet, P.; Guth, J. L.; Hazm, J.; Lamblin, J. M.; Gies, H. *Eur. J. Solid State Inorg. Chem.* **1991**, *28*, 345.

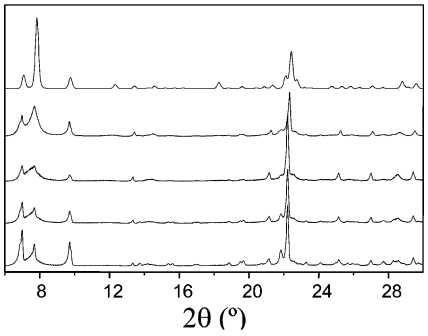

Figure 14. Powder XRD pattern of (from top to bottom) polymorph A (BEA, simulated), a solid obtained using (+)EABO-5 ($H_2O/SiO_2 = 2-3$, 135 °C, 27 days), and the simulation of three physical mixtures of Beta and ITQ-7 (90, 80, and 60% of zeolite Beta, respectively).

of disorder increases.

The lack of stacking faults and the NMR results lead us to postulate that the observed disorder may have a local rather than extended nature. Particularly, given the changes observed in the ^{19}F MAS NMR results we suggest that disorder may be associated with D4R units, which could be occasionally missing or incompletely built. Analysis of the fluoride content of the samples, while showing a large dispersion, indicates a slightly decreased F content as the degree of disorder increases (Supporting Information, Figure 3S). For each missing F anion the existence of a $Si-O^-$ is required for charge balance; hence, at least a connectivity defect must exist. Fluoride-free D4R units, given the strain due to their acute T−O−T angles, would be energetically favorable positions to place such a defect. As further support to this hypothesis, partial substitution of Si by Ge (Si/Ge = 5) under otherwise identical conditions yields materials with an enhanced degree of order (Figure 12). Ge has been proposed to favor the formation of structures with D4R units.[26,33] This has been justified as an effect of the decreased covalent character of T−O bonds and the resultant increased flexibility of TO_4 units in four rings upon introduction of a T element larger and more electropositive than Si.[34] The results presented in Figure 12 apparently point toward the conclusion postulated above, that is, that disorder in ITQ-7 is related to D4R units.

As a result of the evidence that indicates absence of stacking faults in ITQ-7, we investigated the effect of lattice strain broadening (i.e., the presence of a distribution of lattice spacings owing to a distribution of "point" defects in the lattice such as missing atoms or uncondensed silanols). SEM images (Supporting Information, Figure 4S) indicate domain sizes large enough that effects of crystal size broadening are unlikely, hence this feature was not included in the calculations. Figure 13a shows the simulated powder XRD patterns of ITQ-7 with different degrees of lattice strain in the *ab* plane. A detailed comparison of the XRD patterns reveals that the inclusion of *ab* lattice strain qualitatively explains the evolution of almost all the peak broadening features that are observed in the increasingly disordered samples of Figure 5. However, a small number of features are not satisfactorily

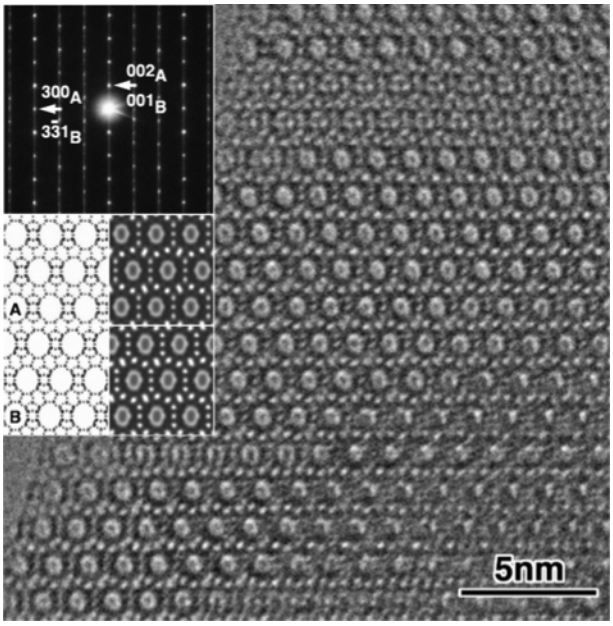

Figure 15. HRTEM image of a crystal of the solid obtained using (+)-EABO-5. The image allows the identification of the crystal as zeolite Beta. The corresponding ED pattern is shown in the upper inset, while the lower inset contains a representation of polymorphs A and B of the Beta structure (labeled A and B, respectively) and their simulated images.

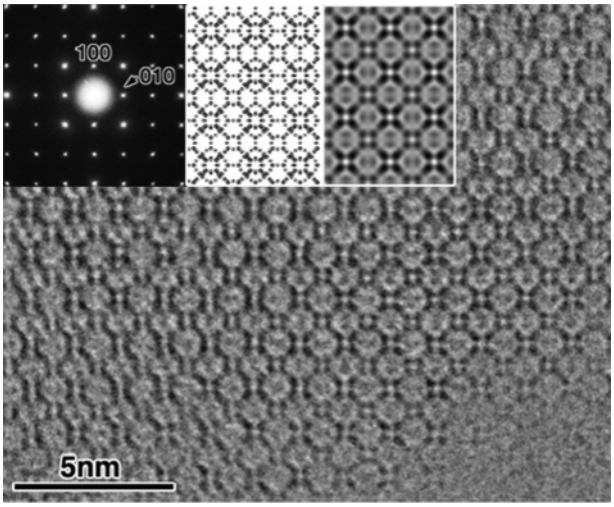

Figure 16. HRTEM image of a different crystal of the solid obtained using (+)EABO-5. The image allows the identification of the crystal as zeolite ITQ-7 (ISV). The corresponding ED pattern is shown in the left inset, while the middle inset contains a representation of the ISV structure and its simulated image.

explained by *ab* lattice strain alone, for example, the cluster of peaks between 19.25 and 20° 2θ and those between 29 and 30° 2θ. Figure 13b shows the effect of strain broadening in the *c* direction. In this case, most of the observed broadening features are not correctly reproduced, although the evolution of the two features mentioned above is now correctly reproduced. Therefore, we conclude that (1) lattice strain broadening certainly has a strong influence on the observed changes in the XRD patterns of ITQ-7 and (2) this strain broadening has a considerable *ab* plane component, although a contribution from the *c* component cannot be ruled out.

A more detailed study of these effects would entail refinement of the crystal structure with inclusion of lattice

(33) Villaescusa, L. A.; Camblor, M. A. *Recent Res. Dev. Chem.* **2003**, *1*, 93.
(34) Blasco, T.; Corma, A.; Díaz-Cabañas, M. J.; Rey, F.; Vidal-Moya, J. A.; Zicovich-Wilson, C. M. *J. Phys. Chem. B* **2002**, *106*, 2634.

strain broadening, refinement of the occupancies of atoms suspected to be involved in the defects that cause the lattice strain broadening, and consideration of the effects of instrumental broadening, to determine their cumulative effect on the shape of the XRD profile. In this paper, we have restricted ourselves to a qualitative explanation of the XRD patterns. However, we may speculate on the nature of the defects causing the strain broadening. As shown in Figure 8, ITQ-7 can be built by connecting the SBU (Figure 8a,b) with oxygen bridges in all three principal crystal directions, thus creating D4Rs in the three principal planes. If the defects (such as missing silicon atoms and/or uncondensed silanols) are in the D4Rs created by the oxygen bridges in the *c* direction, they would mainly cause lattice strain broadening in the *c* direction. The silicon atom involved would be Si4.[21] On the other hand, if the defects are in the D4Rs created by the oxygen bridges in the *a* and *b* directions, then one would expect strain broadening in primarily the *ab* plane. The silicon atoms involved would be Si1 and Si3.[21] While the existence of defects in the interior of the SBU itself, with a more complex effect on the XRD, cannot be ruled out on the basis of these simulations, the experimental results commented on above (^{19}F MAS NMR, F analysis, and synthesis with Ge) all point to defects in D4R units.

Thus, we conclude that the structural disorder in ITQ-7, causing anisotropic broadening in the XRD patterns, may be likely due to point defects (missing Si or connectivity defects) mainly associated to D4R units in the *ab* plane. Given the dependence of disorder on synthesis conditions, with order increasing at a lower water/silica ratio, this may suggest a better selectivity in the structure-directing effect of fluoride at high concentrations. Further work is still needed to elucidate the nature of disorder in ITQ-7 and its dependence on synthesis conditions.

Synthesis with Enantiomerically Enriched EABO-5. The use of chiral organic SDA cations in an attempt to synthesize chiral zeolites is well-justified: a chiral zeolite in enantiomerically pure form could eventually find applications in asymmetric catalysis and separation. Previous uses of chiral cations have been reported in the literature,[2,35−37] with essentially no success toward the goal of crystallizing a chiral silica-based zeolite in pure enantiomeric form. Given that the use of EABO-5 may yield under certain conditions zeolite Beta and recalling that polymorph A of Beta is chiral, we decided to try the synthesis using the EABO-5 enriched in the dextrorotary isomer. Another motivator for this study was our successes at obtaining pure phases as well as intergrowths under different synthesis conditions. Most attempts were made using conditions that would yield zeolite Beta if the racemate were employed, although some experiments in conditions yielding ITQ-7 were also performed. The results, which are summarized in Table 4, are similar to those obtained with the racemate (except for experiments L545, using the enantiomerically enriched cation, and L503, using the racemate, which, intriguingly, gave different results under similar conditions). Generally, the synthesis with the enantiomerically enriched cation yields ITQ-7 at high temperature and low water/silica ratios, with zeolite Beta competing at lower temperature and other intergrown phases appearing at higher levels of dilution. One of the materials deserved, however, special attention since its XRD pattern was similar to that simulated for polymorph A, although it could also be a mixture of Beta and ITQ-7 (Figure 14). Unfortunately, HRTEM and ED of this sample revealed the coexistence of both Beta (Figure 15) and ITQ-7 (Figure 16) with no hints of pure polymorph A. Although it is not possible to exclude the possibility that there was some enrichment in one enantiomer of polymorph A in the crystallized Beta, we have no reason to believe this to be the case.

Conclusions

Several organic cations derived from a rigid bicyclic amine have been used as SDAs in the synthesis of pure silica zeolites at varying water/silica ratios. The smaller and rigid *N*,*N*-dimethyl derivative afforded the synthesis of ITE and STF, both presenting relatively large cages plus small and medium pores, respectively. In contrast, the larger but more flexible *N*,*N*-diethyl cation showed a poor specificity and only led to intergrown structures. With regard to the *N*,*N*-tetramethylene cation, with a five-membered cycle over N, its large size prevented the crystallization of ITE or STF while its relatively large conformational rigidity afforded the synthesis of the new large pore ITQ-7. Similar results were found when using the *N*,*N*-pentamethylene derivative.

The nature of structural disorder in ITQ-7 materials remains elusive, but we have proven by HRTEM and ED that no stacking faults and, hence, no BEC/ISV or other intergrowths exist. The presence of disorder is evidenced not only by XRD powder diffraction of the calcined materials in particular but also by ^{29}Si NMR of the calcined samples and ^{19}F and ^{29}Si MAS NMR and ^{29}Si CP MAS NMR of the as-made samples. The ^{19}F MAS NMR spectra and the enhanced degree of order when Si is partially substituted by Ge suggest a relationship between disorder and D4R units, which could be ocassionally missing or incompletely built in the disordered materials. XRD simulations of strain effects, which could be caused by such point defects, suggest the defects would be mainly associated to D4R units on the *ab* plane.

Acknowledgment. Financial support by the Spanish CICYT (Project Nos. MAT97-0723 and MAT2003-06003-C02-01) is gratefully acknowledged. M.A.C. and L.A.V. thank E. Pérez for assistance in zeolite and SDA syntheses. The authors thank T. Ohsuna for helpful discussions and one reviewer for suggesting the lattice strain simulations.

(35) Nakagawa, Y. U.S. Patent 5,271,922, 1993.
(36) Tsuji, K.; Wagner, P.; Davis, M. E. *Microporous Mesoporous Mater.* **1999**, *28*, 461.
(37) Kubota, Y.; Helmkamp, M. M.; Zones, S. I.; Davis, M. E. *Microporous Mater.* **1996**, *6*, 213.

Supporting Information Available: C, H, and N analysis and ^{1}H NMR spectra of DMABO, DEABO, and EABO, crystallographic data for $C_{14}H_{26}BrN\cdot H_2O$ (EABO-5 racemate), summary of synthesis results using DMABO and EABO as SDAs, powder

XRD and micrographs of intergrown materials MI-2 and MI-3, ^{29}-Si MAS NMR and ^{29}Si CP MAS NMR spectra of the disordered as-made ITQ-7 materials, list of variant and invariant reflections for pure silica ITQ-7 materials, F content in the ITQ-7 samples as a function of disorder, lattice energy minimization results for pure SiO_2 BEC and ISV topologies using the GULP code, and SEM images of ITQ-7 materials with varying degrees of XRD disorder (PDF). Diffax input files for XRD simulations of ISV/BEC intergrowths (a ZIP file comprising six text files named as isv_xx.txt, where xx denotes % of ISV). An X-ray crystallographic file (CIF). This material is available via the Internet at http://pubs.acs.org.

CM0622248